ISSN 1062-8738, Bulletin of the Russian Academy of Sciences: Physics, 2017, Vol. 81, No. 11, pp. 1353–1359. © Allerton Press, Inc., 2017.
Original Russian Text © V.E. Gromov, Yu.F. Ivanov, A.M. Glezer, V.E. Kormyshev, S.V. Konovalov, 2017, published in Izvestiya Rossiiskoi Akademii Nauk, Seriya Fizicheskaya, 2017, Vol. 81, No. 11, pp. 00000–00000.

Electron-Beam Modification of a Surface Layer Deposited on Low-Carbon Steel by Means of Arc Spraying

V. E. Gromov[a, *], Yu. F. Ivanov[b, c], A. M. Glezer[d, e], V. E. Kormyshev[a], and S. V. Konovalov[a]

[a] *Siberian State Industrial University, Novokuznetsk, 654007 Russia*

[b] *Institute of High Current Electronics, Siberian Branch, Russian Academy of Sciences, Tomsk, 634055 Russia*

[c] *National Research Tomsk State University, Tomsk, 634050 Russia*

[d] *Bardin Central Scientific Research Institute of Ferrous Metallurgy, Moscow, 107005 Russia*

[e] *National Research Technological University (MISiS), Moscow, 119049 Russia*

**e-mail: gromov@physics.sibsiu.ru*

Abstract—State-of-the-art means of physical materials science are used to study the structure, phase composition, defect substructure, and tribological properties of a coating formed on low-carbon Hardox 450 martensite steel via the electrocontact deposition of an Fe–C–Ni–B wire and modified through subsequent irradiation with high-intensity pulsed electron beams. It is shown that electron-beam treatment results in the formation of a modified 50-μm thick surface layer, the main phases of which are the α-phase, iron boride FeB, and boron carbide B_4C. In the layer modified by electron-beam treatment, the transverse size of batch martensite crystals is reduced by a factor of 3, relative to the initial Hardox 450 steel, and ranges from 50 to 70 nm. It is established that the wear resistance of the deposited layer after electron-beam treatment grows by more than 20 times with respect to the wear resistance of Hardox 450 steel, and the friction coefficient is reduced by a factor of 3.5. The microhardness of a deposited layer ~7 mm thick is more than double that of the base metal.

Keywords: structure, phase composition, defective substructure, tribological properties, electron-beam treatment of low-carbon martensite steel

DOI: 10.3103/S1062873817110107

INTRODUCTION

The problem of improving the reliability and durability of machines and mechanisms is currently being solved via targeted and controlled changes in the properties of their working surfaces. Obtaining coatings with high functional properties that improve the durability of products under extreme conditions of high wear, corrosion, mechanical loads, and temperature, is an important fundamental problem [1]. The most promising ways of hardening and reducing that allow us to drastically improve the properties of surfaces are the cost-effective techniques of surfacing [2–4], since the service life of parts is determined mainly by the durability of coatings. The main factors that determine their functional properties are the chemical and phase compositions of the coating material.

The formation of Fe_2B borides on surfaces of the ASTM A-36 steel widely used in the metalworking and petrochemical industries results in a 400 to 500% increase in hardness and corrosion resistance [5]. Additions of boron-containing powder for the deposition of Fe–Cr–C coatings with mixtures of powder (F–Cr, cast iron, stainless steel) allow us to form pre-eutectic and hypereutectic alloys, and thus to vary their functional properties [6]. The authors of [7] proposed a new composition for an Fe–Cr–S–B flux-cored wire used to form high-temperature corrosion-resistant coatings. Compared to the Fe–Cr and Ni–Cr–Ti coatings used traditionally, this deposited layer has the greatest microhardness and corrosion resistance in a solution of Na_2SO_4 + 25% K_2SO_4 at 650°C.

To properly select coating materials that correspond to conditions of operation, we must perform detailed studies of their properties and structure [8–11]. At the same time, special attention must be given to relationships between tribological properties and microstructure for designated products operating under conditions of severe wear [5–7].

The aim of this work was to analyze the results obtained by studying the structure, mechanical, and tribological properties of a layer formed on Hardox 450 steel via electrocontact deposition with an Fe–C–Ni–B flux-cored wire and modified by a high-intensity pulsed electron beam.

EXPERIMENTAL

We used Hardox 450 steel as our base material (content, mass %: 0.19 C; 0.70 Si; 1.6 Mn; 0.025 P; 0.010 S; 0.25 Cr; 0.25 Ni; 0.25 Mo; and 0.004 B; the

remainder was Fe). It was characterized by a low content of alloying elements, and was therefore easily welded and processed. A fine-grained structure and a high degree of hardness can be achieved in the steel using a special quenching system that includes the rapid cooling of a rolled sheet without subsequent tempering. The steel is then especially resistant to most types of wear. The hardened layer was deposited via MIG/MAG (Metal Inert Gas/Metal Active Gas) arc welding, using melting metal electrodes with an automatic feed of filler wire in a gas environment (Ar = 98%, CO_2 = 2%), welding currents that ranged from 250 to 300 A, and voltages of 30–35 V. As the electrode for deposition, we used a flux-cored wire with a chemical composition (mass %) of 0.7 C; 2.0 Mn; 1.0 Si; 2.0 Ni; and 4.5 B; the remainder was Fe.

The deposited layer was modified by irradiating the surface in two stages with the high-intensity electron beam of the SOLO facility [12] in the mode of melting and high-rate crystallization. At the first stage, the electron beam had the following parameters: energy density E_S of the electron beam per unit pulse, 30 J cm^{-2}; pulse duration τ, 200 μs; number N of pulses, 20. At the second stage, E = 30 J cm^{-2}; τ = 50 μs; and N = 1. The modes of irradiation were chosen based on calculations of the temperature field formed in the surface layer of the material upon irradiation in the single-pulse mode [13]. The modified surface was subjected to tribological testing using a high-temperature S/N 07-142 unit (CSEM Instruments). A ball 2 mm in diameter and made of hard VK6 alloy was used as the counterbody. The rate of wear was estimated from the area of the cross section of the wear track using a STIL MICRO MEASURE 3D profilometer station.

The bulk structure of the modified layer was analyzed using a transverse cross section technique in which samples were cut into two parts, perpendicular to the modified surface. The defective structure of the material was studied by means of optical microscopy, using a μVizo-MET-221 metallographic microscope; scanning electron microscopy, using a Philips SEM-515 electron microscope; and transmission electron diffraction microscopy, using EM-125 FET and Tecnai 2062 TWIN electron microscopes [14–17]. The elemental composition of the surface layer was determined via microprobe X-ray analysis using an EDAX ECON IV microanalyzer (an attachment for a Philips SEM-515 scanning electron microscope). The phase composition of the surface layer was analyzed by means of X-ray diffraction, using a Shimadzu XRD-7000s diffractometer (Japan) [18, 19].

RESULTS AND DISCUSSION

Bulk Structure of the Workpiece

Hardox 450 grade steel is designed to operate under conditions in which special requirements are imposed for wear resistance in combination with good cold bending and good weldability. The steel's high degree of hardness is achieved using a special sheet quenching system with which the metal acquires a martensite structure.

The formation of a layer on the steel via electric arc deposition is accompanied by poorly controlled heating of the material. This tempers the quenched state. The tempering of the steel separates the particles of the carbide phase (cementite) in the bulk of the plates and at their boundaries. The particles have the acicular shape characteristic of the cementite formed during the low-temperature tempering of hardened steel [20, 21]. The defective substructure of the martensite plates takes the form of dislocations. The dislocations are either chaotically arranged or form a reticulate substructure. The scalar density of dislocations varies over a very wide range: 3×10^9 to 6.5×10^{10} cm^{-2}. It should be noted that the crystals of martensite characteristic of hardened steel exhibit a scalar dislocation density of 10^{11} cm^2 [21, 22]. The heating of the steel is accompanied by the destruction of the martensite crystals' boundaries, which is especially characteristic of batch martensite.

Structure of the Contact Layer

We shall define the contact layer as the metal layer at the interface between the deposited layer and the bulk of the material. On the side of the base metal (Hardox 450 steel) was a polycrystalline structure, in the bulk of whose grains we observed a lamellar-type substructure (Fig. 1a). The plates were grouped into batches; the transverse size of the plates ranged from 150 to 200 nm. The high values of the scalar density of dislocations ($\approx 4.8 \times 10^{10}$ cm^{-2}) and the grouping of plates into batches indicate a martensite (shear) mechanism of their formation.

Particles belonging to the second phase were found in the bulk and at the boundaries of the plates (Fig. 1b). Microdiffraction analysis revealed reflexes that belonged mainly to iron carbide (cementite). The particles had a globular shape; their size ranged from 20 to 30 nm. It should be noted that the cementite particles in hardened steel have a lamellar (acicular) shape [20, 21]. A structure of tempered martensite therefore formed on the substrate side in the zone of contact between the deposited layer and the substrate's metal. Along with the structure of the tempered martensite, there were grains in the zone of contact and the joints of the boundaries. Along the edges of the boundaries, we observed extensive interlayers of the second phase (Fig. 2).

Dark-field analysis with subsequent indexing of the electron diffraction pattern showed that the formed particles were iron boride FeB (Figs. 2b, 2c). This means that as the deposited layer formed, the bulk of the adjacent steel layer was doped with the elements of the flux-cored wire. The alloying elements (especially

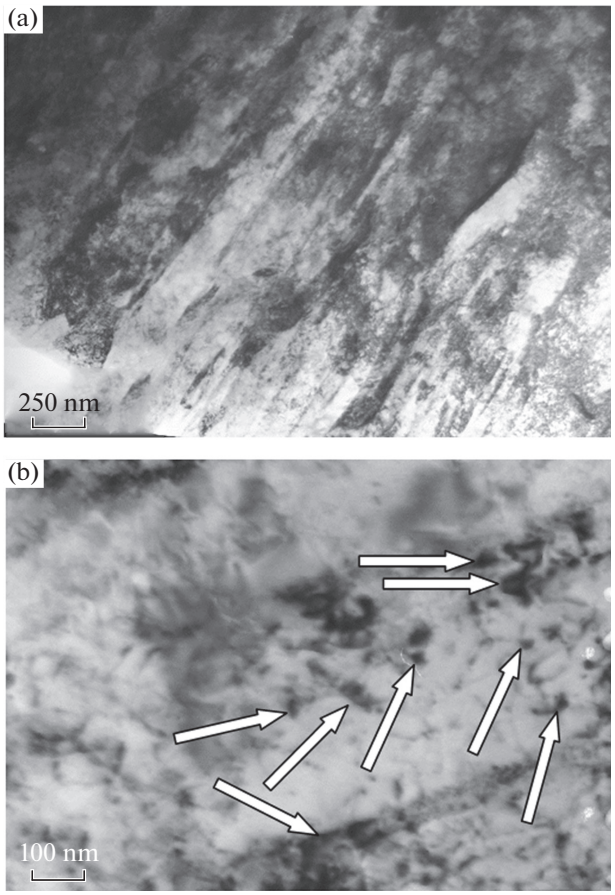

Fig. 1. Structure of the contact layer on the side of Hardox 450 steel. The arrows indicate particles of the second phase.

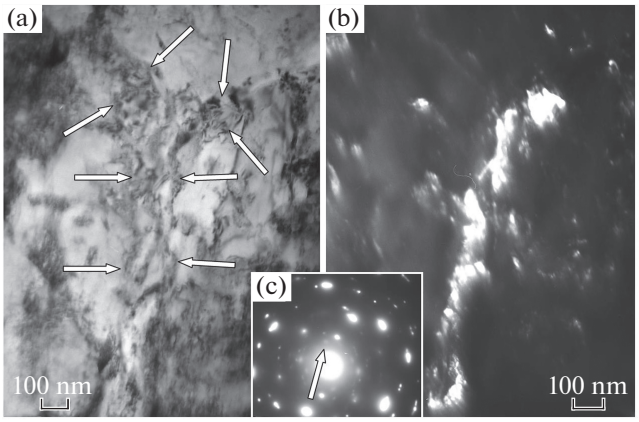

Fig. 2. Electron microscope image of the structure of Hardox 450 steel in contact with the surface layer: (a) bright field image; (b) dark field image obtained in reflex [101] of FeB; (c) micro–electron diffraction pattern (the arrow indicates the reflex in which the dark field image was obtained); in Fig. (a), the arrows indicate FeB particles at the junction between three grains of the α-phase.

boron) diffused predominantly along grain boundaries, leading to the formation of iron boride particles.

A lamellar eutectic structure formed on the side of the deposited layer in the zone of contact. The indexing of the electron diffraction patterns obtained for this structure showed that the eutectic was formed by α-iron and iron boride Fe_2B.

In most cases, the α-phase that formed the eutectic of the contact layer had the structure characteristic of batch martensite. The transverse size of the martensite crystals ranged from 50 to 100 nm, considerably less (by a factor of 3 to 4) than that of the batch martensite crystals detected in the bulk of Hardox 450 steel. The main reason for such a wide dispersal of the batch martensite structure of the contact layer was apparently the thinness (0.5 to 0.8 μm) of the iron interlayers in the eutectic, which underwent a martensite $\gamma \rightarrow \alpha$ transformation during crystallization and subsequent cooling.

Structure of the Surface Layer

A distinctive feature of the phase composition of the surface layer was the formation of iron boride (predominantly Fe_2B) plates in the eutectic. The inclusions of iron boride had no dislocation substructure in their bulk, distinguishing them fundamentally from the adjacent layers of the α-phase. The reason for there being no dislocation substructure in iron boride plates is their comparatively high level of hardness (12.5 to 16.5 GPa) [23, 24]. A characteristic feature of the electron microscopic image of borides is the large number of flexural extinction contours in the bulk of inclusions.

The flexural extinction contours indicate the formation of internal fields of stresses in the material that bent or twisted the crystal lattice [14–17]. The sources of the stress fields (stress concentrators) were boundaries of two types: interphase (interfaces between boride and α-phase inclusions) and intraphase (interfaces between iron borides).

The α-phase that separated the plates of iron boride was mainly martensite of batch morphology, with the transverse size of the plates ranging from 30 to 70 nm. A reticulate-type dislocation substructure was observed in the bulk of the plates. Judging from the size of the cells of dislocation reticles, the scalar density of dislocations was 10^{11} cm^{-2}. The high density of dislocations and the lamellar morphology of the interlayer structure indicate a martensite mechanism was responsible for the formation of the α-phase and the superfine martensite structure. It should be noted for purposes of comparison that with hardened steel, the average transverse size of batch martensite plates ranges from 150 to 200 nm, with the transverse size of the lamellar martensite being as high as several μm [20–22].

Our studies of the structure and phase composition of the deposited layer thus revealed the formation of a

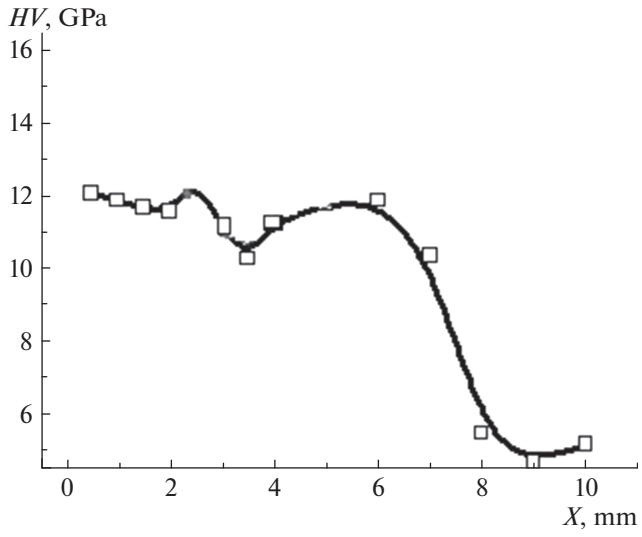

Fig. 3. Microhardness profile of the surface layer–steel system.

multiphase state characterized by a large number of iron boride inclusions whose hardness was more than an order of magnitude greater than that of Hardox 450 steel. It is obvious that the hardness of the eutectic would differ from that of iron boride; indeed, mechanical testing of the material confirmed this assumption.

In analyzing the change in microhardness over the transverse cross section (Fig. 3), we noted the formation of a high-strength surface layer whose microhardness ranged from 10.5 to 12.5 GPa, i.e., more than double the hardness of the base metal (Hardox 450 steel) at a thickness of the deposited layer of at least 7 mm.

Irradiating the deposited layer with a high-intensity pulsed electron beam resulted in a modified surface layer up to 50 μm thick (Fig. 4a, layer 1). The modified layer differed from the bulk of the deposited material in the level of structural dispersion revealed by ion etching of the transverse cross section. Comparing the images of the deposited layer's structure shown in Figs. 4b, 4c, we can see that the irradiation of the deposited material by the intense pulsed electron beam was accompanied by the formation of a structure with etching elements (obviously refractory compounds with a relatively low level of etching by the ion beam) ranging from 200 nm to 500 nm in size (Fig. 4b). In the bulk of the deposited layer not irradi-

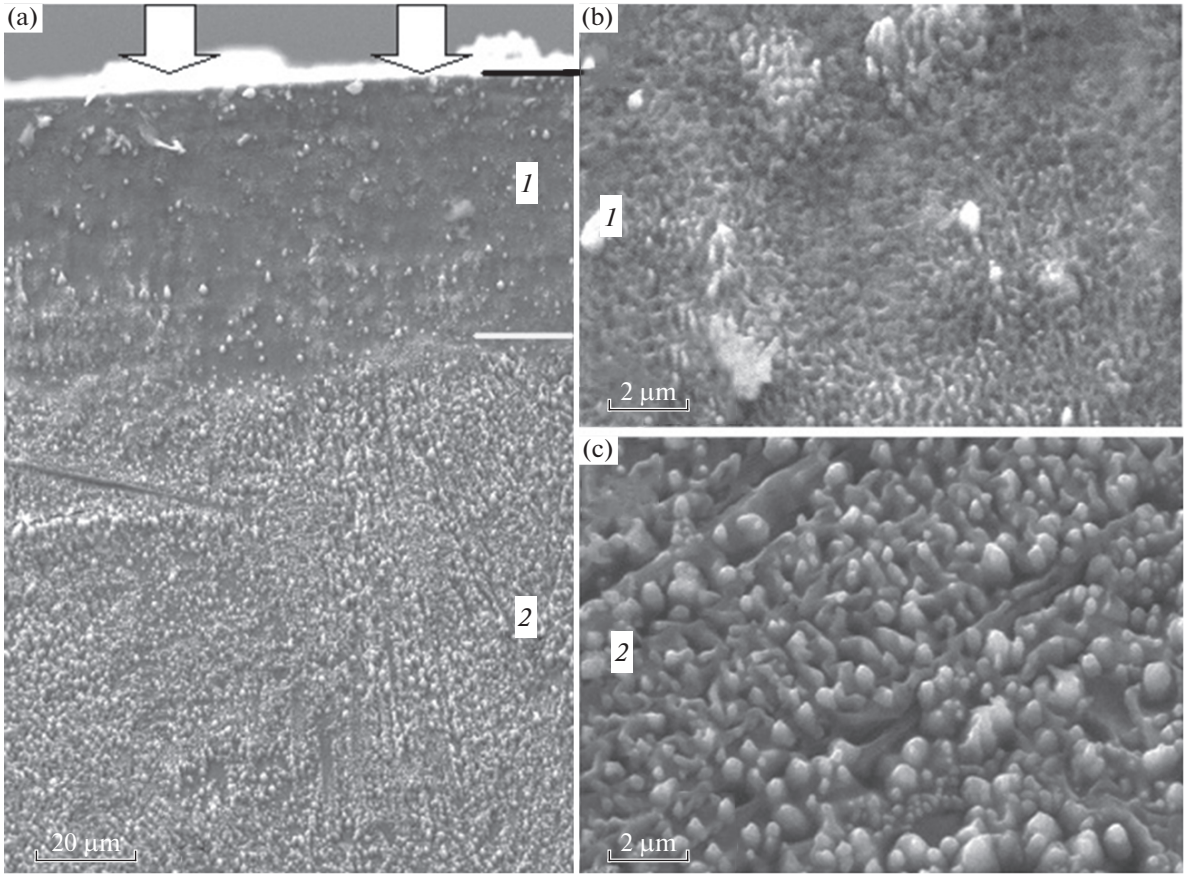

Fig. 4. Structure of a surface layer (an etched transverse cross section). The arrows indicate the surface of the surface layer irradiated by an intense pulsed electron beam. Shown are (*1*) the layer modified by the electron beam; (*2*) the bulk of the surfacing.

ated with the electron beam (Fig. 4a, layer 2), the size of the structure's etched elements is as high as 1.0 μm (Fig. 4c).

The irradiation of the deposited layer's surface substantially alters the phase composition and defect substructure of the material. The considerable reduction in the transverse size of the martensite crystals is especially notable (Fig. 5). If the average transverse size of the crystals in the batch martensite ranged from 150 to 200 nm in the steel hardened using a heating furnace [14], the transverse size of the batch martensite crystals ranged from 50 to 70 nm in the deposited layer modified via electron-beam treatment (Fig. 5b). One reason for this change in the transverse size of martensite crystals could be the ultrahigh (up to 10^6 K s^{-1}) cooling rate of the surface layer irradiated by the intense pulsed electron beam. Another possible reason could be that there were small γ-phase volumes between the inclusions of the second phase (Fig. 5a). The deposited surface layer irradiated by the intense pulsed electron beam was a multiphase material.

Note in particular that there was a relatively high content of second phase inclusions. The inclusions in the surface layer had a variety of shapes and were no greater than 1–1.5 μm in size. The phase composition of the modified deposited layer was studied via dark-field microdiffraction analysis. The results showed the surface layer contained phases FeB (Fig. 6a) and B_4C (Fig. 6c).

Electron diffraction microscopy thus demonstrated that the deposited surface layer modified by an intense pulsed electron beam was a multiphase aggregate whose main phases were a solid solution based on α-iron, iron boride FeB, and boron carbide B_4C. The additional presence of such iron carbides (carboborides) as Fe_3C or $Fe_3(C, B)$ cannot be excluded.

The formation of a deposited layer improves the wear resistance of steel. Our tests showed that the wear resistance of our deposited layer modified using an intense pulsed electron beam was more than 20 times that of steel, and more than 11 times that of the deposited layer not modified by the electron beam (Table 1). The friction coefficient of the deposited layer after irradiation with the electron beam fell considerably. For the initial steel, this value was 0.31; for the deposited layer, it was 0.14. After irradiating the deposited layer with the electron beam, the friction coefficient was 0.09.

Figure 7 shows the change in the friction coefficient during the tribological testing of the deposited layer modified using the electron beam. The two-stage character of the change in the friction coefficient should be noted. At the first stage, the friction coefficient was approximately 0.07; at the second stage, it was around 0.11. The friction coefficient of steel without surfacing was around 0.31. Analyzing the change in the friction coefficient during tribological testing (Fig. 7), we may assume that irradiating the deposited layer with an intense pulsed electron beam considerably reduced (by a factor of 3.5) the friction coefficient of the deposited layer.

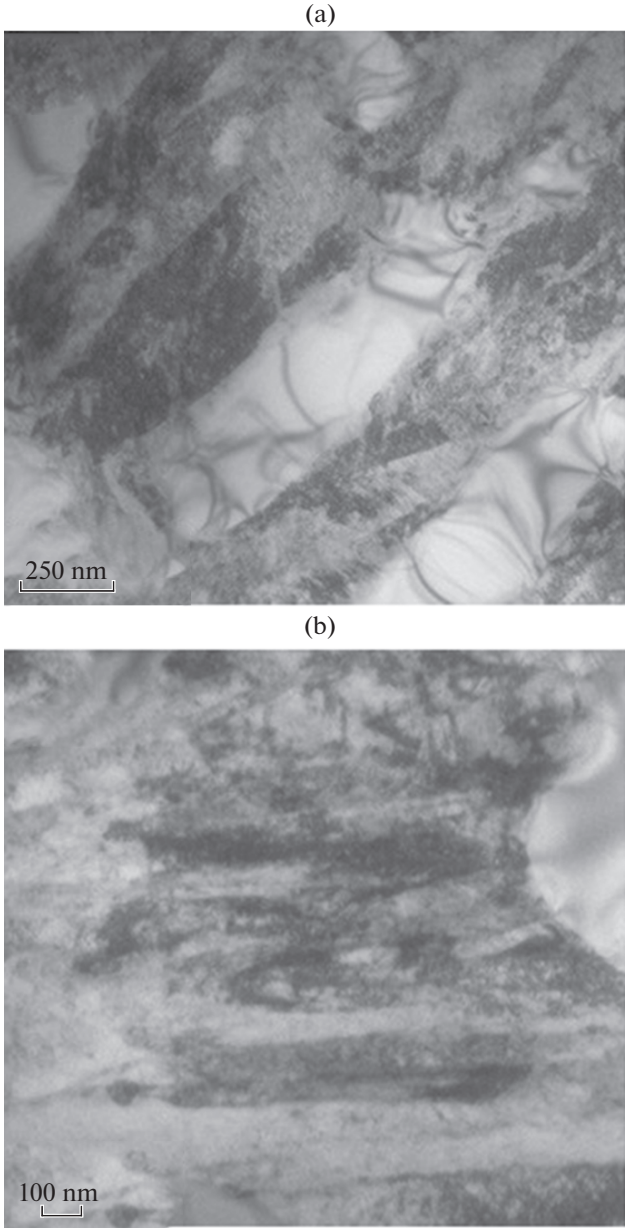

Fig. 5. Electron microscope image of the structure of the α-phase (the solid solution based on iron's bcc crystal lattice) formed as a result of the fast cooling of the top layer of a surface irradiated by an intense pulsed electron beam.

Table 1. Results from tribological testing

	Friction coefficient	Wear rate
Hardox 450 steel	0.31	5.4
Surface layer	0.14	2.8
Surface layer after electron-beam treatment	0.09	0.24

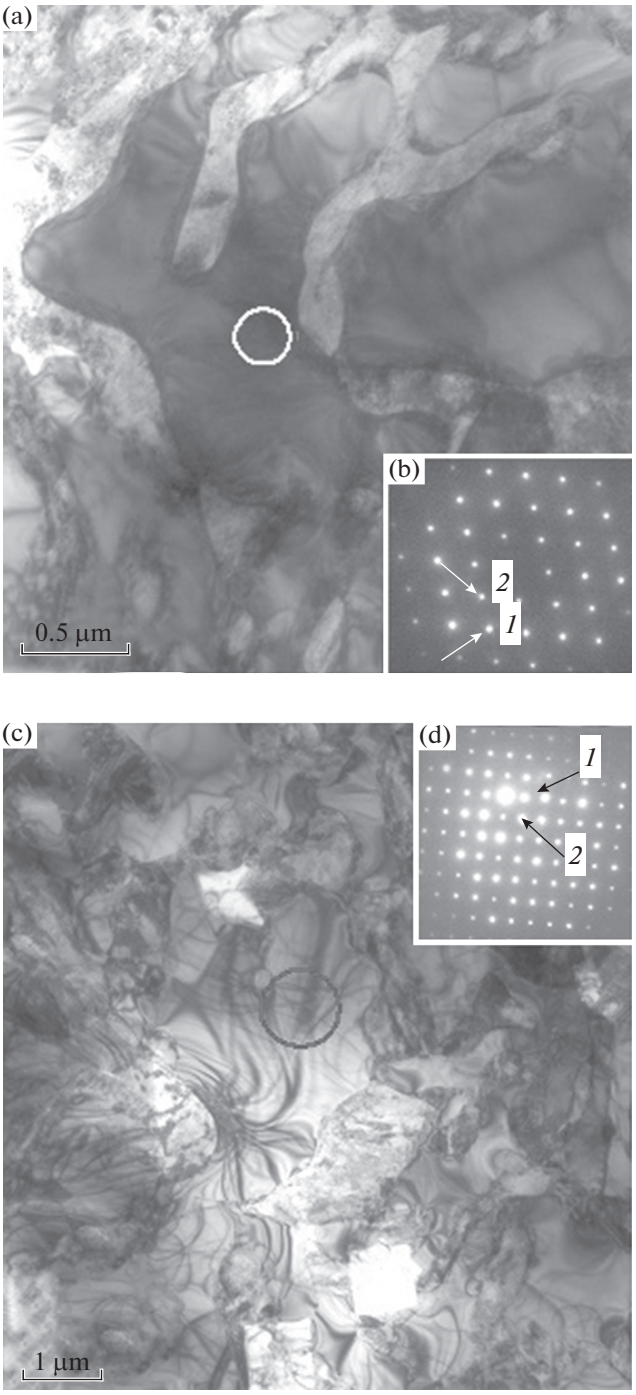

Fig. 6. Electron microscope image of the deposited layer superficial structure after electron-beam treatment: (a) bright field image; (b, c) bright field images, (b, d) micro-electron diffraction patterns obtained from regions highlighted by the circles in Figs (a) and (c). The arrows in (b) indicate the reflexes of the FeB phase: (*1*) [011]; (*2*) [111]. The reflexes of phase ~~B4C~~ are indicated in (d): (*1*) [012]; (*2*) [110].

CONCLUSIONS

The phase composition, defect substructure, and tribological properties of a layer formed on Hardox steel via the electrocontact deposition of Fe–C–Ni–B wire, modified by irradiating it with a high-intensity pulsed electron beam, were studied. It was shown that electron-beam treatment of a deposited layer results in the formation of a multiphase state, the main phases of which are an α-phase (a solid solution based on the bcc crystal lattice of iron), iron boride FeB, and boron carbide B_4C.

It was found there are flexural extinction contours that indicate the formation of internal stress fields at the interfaces between phases FeB and α-Fe. The wear resistance of the surface of the deposited layer after electron-beam treatment was more 20 times greater than that of the initial Hardox 450 steel, while the friction coefficient was lower by a factor of 3.5.

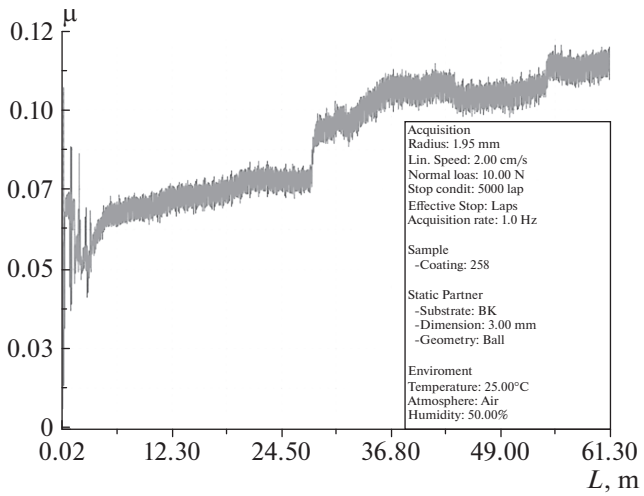

Fig. 7. Friction coefficient μ, depending on track length *L* in tribological testing. The insert shows the conditions of our tribological tests.

ACKNOWLEDGMENTS

This work was supported by the Russian Science Foundation, project no. 15-19-00065. The electron-beam treatment of the surface layer was performed with the support of the Russian Foundation for Basic Research, project no. 16-49-700659 p_a.

REFERENCES

1. Kapralov, E.V., Budovskikh, E.A., Gromov, V.E., et al., *Struktura i svoistva kompozitsionnykh iznosostoikikh naplavok na stal'* (Structure and Properties of Composite Wear-Resistant Weld Deposits on Steels), Novokuznetsk: Sib. Gos. Ind. Univ., 2014.
2. Kapralov, E.V., Raykov, S.V., Budovskikh, E.A., Gromov, V.E., Vashchuk, E.S., and Ivanov, Yu.F., *Bull. Russ. Acad. Sci.: Phys.*, 2014, vol. 78, no. 10, p. 1015.
3. Gromov, V.E., Kapralov, E.V., Raykov, S.V., et al., *Usp. Fiz. Met.*, 2014, vol. 15, p. 211.

4. Popova, N.A., Nikonenko, E.N., Ivanov, Yu.F., et al., *Adv. Mater. Res.*, 2014, vol. 1013, p. 194.
5. Marquez-Herrera, A., Fernandez-Munoz, J.L., Zapata-Torres, M., et al., *Surf. Coat. Technol.*, 2014, vol. 254, p. 433.
6. Zahiri, R., Sundaramoorthy, R., Lysz, P., and Subramanian, C., *Surf. Coat. Technol.*, 2014, vol. 260, p. 220.
7. Li, R., Zhou, Z., He, D., et al., *J. Therm. Spray Technol.*, 2015, vol. 24, no. 5, p. 857.
8. Yüksel, N. and Şahin, S., *Mater. Des.*, 2014, vol. 58, p. 491.
9. Venkatesh, B., Sriker, K., and Prabhakar, V.S., *Proc. Mater. Sci.*, 2015, vol. 10, p. 527.
10. Gualco, A., Marini, C., Svoboda, H., and Surian, E., *Proc. Mater. Sci.*, 2015, vol. 8, p. 934.
11. Teker, T., Karatas, S., and Osman Yilmaz, S., *Prot. Met. Phys. Chem. Surf.*, 2014, vol. 50, no. 1, p. 94.
12. Koval', N.N. and Ivanov, Yu.F., *Russ. Phys. J.*, 2008, vol. 51, no. 5, p. 505.
13. *Evolyutsiya struktury poverkhnostnogo sloya stali, podvergnutoi elektronno-ionno-plazmennym metodam obrabotki* (Evolution of the Structure of the Surface Layer of Steel Subjected to Electron-Ion-Plasma Treatment), Koval', N.N. and Ivanov, Yu.F., Eds., Tomsk: NTL, 2016.
14. Utevskii, L.M., *Difraktsionnaya elektronnaya mikroskopiya v metallovedenii* (Diffraction Electron Microscopy in Metallography), Moscow: Metallurgiya, 1973.
15. Andrews, K.W., Dyson, D.J., and Keown, S.R., *Interpretation of Electron Diffraction Patterns*, Springer, 1967.
16. *Practical Methods in Electron Microscopy*, Glauert, A.M., Ed., Amsterdam: North Holland, 1972.
17. Smirnova, A.V., Kokorin, G.A., and Polonskaya, S.M., *Elektronnaya mikroskopiya v metallovedenii* (Electron Microscopy in Metallography), Moscow: Metallurgiya, 1985.
18. Brandon, D. and Kaplan, W.D., *Microstructural Characterization of Materials*, Wiley, 2008.
19. Krishtal, M.M., Yasnikov, I.S., and Polunin, V.I., *Skaniruyushchaya elektronnaya mikroskopiya i rentgenospektral'nyi mikroanaliz v primerah prakticheskogo primeneniya* (Scanning Electron Microscopy and Electron Microprobe Analysis: Application Examples), Moscow: Tekhnosfera, 2009.
20. Kurdyumov, G.V., Utevskii, L.M., and Entin, R.I., *Prevrashcheniya v zheleze i stali* (Transformations in Iron and Steel), Moscow: Nauka, 1977.
21. Ivanov, Yu.F., Kornet, E.V., Kozlov, E.V., and Gromov, V.E., *Zakalennaya konstruktsionnaya stal': struktura i mekhanizmy uprochneniya* (Hardened Structural Steel: Structure and Hardening Mechanisms), Novokuznetsk: Sib. Gos. Ind. Univ., 2010.
22. Petrov, Yu.N., *Defekty i bezdiffuzionnoe prevrashchenie v stali* (Defects and the Diffusionless Transformation in Steel), Kiev: Naukova Dumka, 1978.
23. Samsonov, G.V., Serebryakova, T.I., and Neronov, V.A., *Boridy* (Borides), Moscow: Atomizdat, 1975.
24. Kuz'ma, Yu.B. and Chaban, N.F., *Dvoinye i troinye sistemy, soderzhashchie bor* (Boron-Containing Binary and Ternary Systems), Moscow: Metallurgiya, 1990.

Translated by O. Polyakov

SPELL: 1. ok